Ann. Geophys., 26, 2929–2936, 2008
www.ann-geophys.net/26/2929/2008/

Annales Geophysicae

Energetics and structure of the lower E region associated with sporadic E layer

K.-I. Oyama[1], **K. Hibino**[2], **T. Abe**[3], **R. Pfaff**[4], **T. Yokoyama**[5,*], **and J. Y. Liu**[1]

[1]Institute of Space Science, National Central University, NO300, Jhongda Rd., Jhongli City, Taoyuan, Taiwan, China
[2]Faculty of Science, University of Tokyo, Hongo, Bunnkyo-Ku, Tokyo, Japan
[3]Institute of Space and Astronautical Science, JAXA, 3-1-1, Sagmihara, Kanagawa, Japan
[4]NASA Goddard Space Flight Center, Greenbelt, MD, USA
[5]Solar Terrestrial Environment Laboratory, Nagoya University, Aichi, Japan
[*]now at: Earth and Atmospheric Sciences, Cornell University, Ithaca, NY, USA

Received: 14 January 2008 – Revised: 4 August 2008 – Accepted: 11 August 2008 – Published: 25 September 2008

Abstract. The electron temperature (T_e), electron density (N_e), and two components of the electric field were measured from the height of 90 km to 150 km by one of the sounding rockets launched during the SEEK-2 campaign. The rocket went through sporadic E layer (E_s) at the height of 102 km–109 km during ascent and 99 km–108 km during decent, respectively. The energy density of thermal electrons calculated from N_e and T_e shows the broad maximum in the height range of 100–110 km, and it decreases towards the lower and higher altitudes, which implies that a heat source exists in the height region of 100 km–110 km. A 3-D picture of E_s, that was drawn by using T_e, N_e, and the electric field data, corresponded to the computer simulation; the main structure of E_s is projected to a higher altitude along the magnetic line of force, thus producing irregular structures of T_e, N_e and electric field in higher altitude.

Keywords. Ionosphere (Electric fields and currents; Ionospheric irregularities; Mid-latitude ionosphere)

1 Introduction

The SEEK-2 campaign was planned in order to study the sporadic E layer, which accompanies quasi-periodic (QP) echoes with two sounding rockets launched from the Kagoshima Space Center (Geographic location; 131°05′ E, 31°15′ N). The campaign was conducted when two radars were set up at the temporary stations at the north and south of Tanegashima Island (Saito et al., 2005) to observe QP echoes. These were the Lower Thermosphere Profile Radar (130.96° E, 30.38° N); and the Frequency Agile Radar (131.03° E, 30.75° N), respectively. Details of the SEEK-2 campaign and experiment objectives are found in Yamamoto et al. (2005).

One of the rockets, S-310-31, was launched at 23:24 JST on 3 August 2002, containing a glass-sealed Langmuir probe to measure T_e and N_e, an impedance probe to measure N_e, and an electric field probe.

In the past, E_s was examined mainly by using the height profile of N_e, which were obtained by Langmuir probe (Langmuir and Motto-Smith, 1924). Valenzuela et al. (1981) conducted a balloon observation to get the 3-dimensional (3-D) structures by detecting resonance scattering from magnesium ions, which are major ion constituents of E_s. However, nobody was successful in drawing a 3-D structure by sounding rockets as well as from ground observations. Furthermore, a study on energetics in the height region of E_s is a difficult task because of the small number of measurements of T_e in E_s layer have been reported in the past and accuracy is difficult. As far as we know, the paper by Schutz et al. (1976) briefly investigated the energetics of E_s.

In this paper, we discuss the energetics in the lower E region and attempt to draw 3-dimensional structures of E_s, by using T_e, N_e and electric field data that were simultaneously obtained by the rocket.

The outline of this paper is as follows. We first describe the instrumentation of the Langmuir probe and the electric field probe. We then introduce the data in detail. We further discuss the energetics of E region associated with E_s by using the data that has been analyzed. Finally, we speculate what the 3-D structure of E_s is, by using the height profiles of T_e, N_e, and electric field.

Correspondence to: K.-I. Oyama
(oyama@jupiter.ss.ncu.edu.tw)

Published by Copernicus Publications on behalf of the European Geosciences Union.

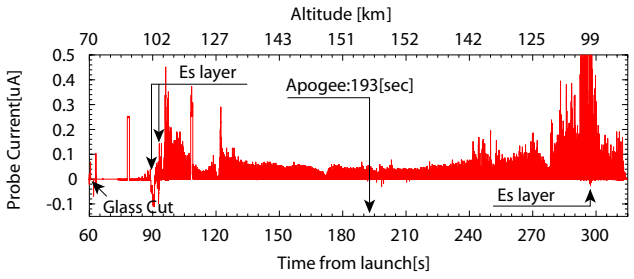

Fig. 1. Currents of the probe biased at 0 V and 2.5 V during rocket flight versus time (from 70 s after rocket launch). Small negative current (ion current), which flows to the probe biased at 0 V starts to appear at 73 s. Positive current of the probe biased at 2.5 V is electron current. Please note, that during 87 s–92.5 s, large ion current is detected and a very small electron current is measured due to the high negative potential of the rocket in the E_s layer.

2 Instrumentation and flight details

As the detail of the Langmuir probe measurement is described in the separate paper (Oyama et al., 2008), a brief description is presented here to provide the information.

The cylindrical electrode of the Langmuir probe is vacuum-sealed in a glass tube after the baking (Oyama and Hirao, 1976). The glass tube is then removed before any measurements of T_e and N_e start in the ionosphere.

The duration of the triangular sweep voltage is 0.25 s and, therefore, one v-i characteristic curve is obtained every 0.125 s. The output voltages of Gain L and H are sampled with 400 Hz and digitized with an 8-bit AD converter. The output voltage of Gain M is sampled with 3200 Hz and digitized with an 8-bit analog-digital converter. These 3 channels are then transmitted to the ground station by real time. The M gain data, which is obtained between 78 s and 108 s after the rocket launch, is sampled by 6400 Hz and digitized with a 12-bit analog-digital converter. The data is stored in memory and at 193 s after the rocket launch, the data transmission is initiated by using M gain channel and completed at 313 s after the launch. Therefore, the real time M gain signal that is sampled with 400 Hz is not available during 193 s and 313 s. This dual sampling allows us to check the effect of the sampling rate as well as the effect of digitization on the T_e calculation.

To measure the electric field of both DC and AC components, a dual set of orthogonal double probes of 4.0 m (tip-to-tip) length is provided. Spherical sensors, with a 4.4 cm diameter, are used to gather the potentials which are detected by high impedance ($>10^{12}\ \Omega$) preamplifiers, using the floating (unbiased) double probe technique. The potential differences on the two main orthogonal axes are digitized on board using 16-bit analog-digital converters, sampled at 1600 samples/s with anti-aliasing filters at 800 Hz (Pfaff et al., 2005).

Figure 1 shows the minimum and maximum probe currents, which correspond to the ion and electron currents to the probe voltage of 0 V and 2.5 V, respectively, for the whole rocket trajectory versus time. The time and altitude of the rocket are marked, respectively, at the bottom and top of the figure from the cut on the glass tube 60 s after the rocket launch. The altitude of the rocket at 60 s after the launch is 70 km. The data is plotted every 0.25 s and 0.125 s for electrons and ion currents, respectively. As Fig. 1 shows, negative current starts appearing from approximately 73 s. At 78 s, the whole measurement system, including current and differential amplifiers, is calibrated. During the time period of 87–92.5 s, the probe current reveals large ion current, which reaches approximately $-0.1\ \mu$A. Expanded v-i current characteristic curves show that the potential of the rocket, with respect to the ambient plasma, drops lower than -2.5 V. As the maximum sweep voltage of the probe is 2.5 V, N_e is not available from the electron current.

The rocket reaches the maximum height of 152 km at 193 s after the launch. During the descent, the most dense E_s layer is detected at 297 s. The T_e and N_e are obtained by semi-log.plotted electron current, which is derived when the ion current is subtracted from the v-i characteristic curve. Since the subtraction of ion current from the v-i current characteristic curve influences the evaluation of the electron temperature, we have developed the human-computer interactive program, which allows us to choose the most probable linear line to the ion current region. Each curve is examined manually and then, finally, the electron current is obtained. The electron current is plotted on a semi-logarithmic scale (logarithmic current versus probe voltage) and only one line, which fits best, is chosen. Finally, the electron temperature is calculated from the slope. This time and energy-consuming procedure is repeated for all v-i curves, both for ascent and descent of the rocket.

3 Results

3.1 Overview of height profiles of T_e and N_e

Figure 2 shows a height profile of N_e, calculated from a DC Langmuir probe for ascent (left panel), and descent (right panel) of the rocket. N_e in the height range of 100–105 km is not shown here, as the detailed discussion on the T_e in the E_s layer, is treated in another paper (Oyama et al., 2008). N_e below the height of 105 km, which is used in Sect. 3.3 to discuss energetics, is obtained by normalizing the electron current that was measured by using the fixed bias spherical probe, with ionosonde. Thus, the N_e data obtained corresponds with data obtained with an impedance probe onboard the same rocket.

At the height of 127 km, N_e starts to fall at 128 km and peaks at 129 km, and then decreases at the height of 129.5 km. Similar features are also found in the electron current obtained with a fixed-bias spherical Langmuir probe (see

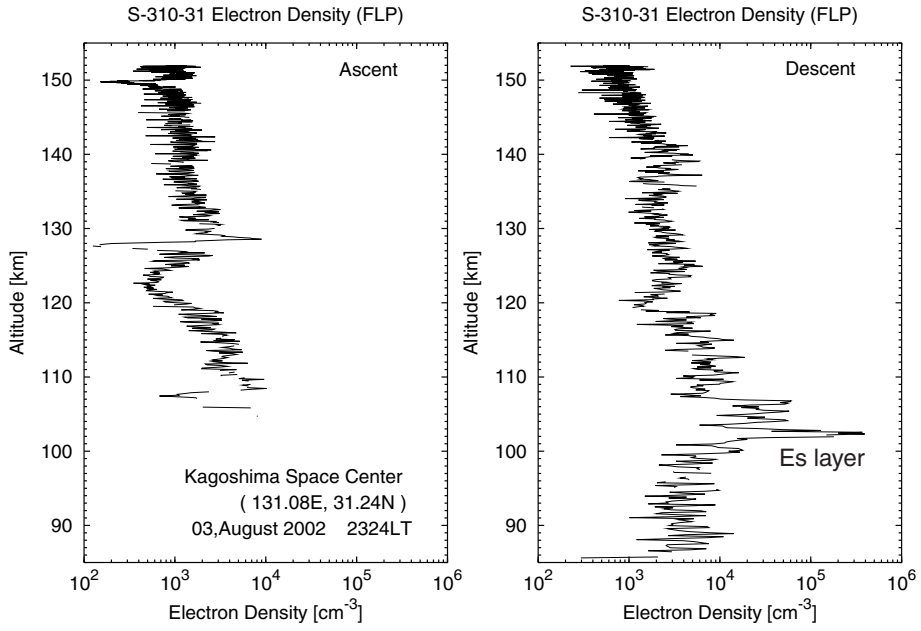

Fig. 2. Height profile of electron density for ascent (left) and descent (right). Data below the height of 106 km during up leg was not available by a glass-sealed Langmuir probe.

Fig. 3, Oyama et al., 2008). The height profile during descent indicates a small E_s at the height of 100–107 km.

Figure 3 shows a height profile of T_e for ascent (left) and descent (right). Neutral temperature, which is calculated from a MSIS-86 model, is also included (Hedin, 1987). It is noted that T_e around the heights of 100 km, is much higher than modelled neutral temperature.

Heights, which show an unusual feature, are marked as 1, 2, 3, 4, 5, and 6 in Fig. 3. First irregular feature appears at the height of 127.5 km (at the height 1) with a strong jump of T_e to 2500 K. At the heights of 139 km and 149.5 km which correspond to the heights 2, and 3, respectively, small spikes of T_e are recognized. At the height of 152 km marked as 4, a small and sharp increase of T_e exists. In addition to these 4 height regions, T_e is found to increase up to about 1400 K at the heights of 119 km–126 km.

During descent, two peaks of T_e are found at the heights of 133 km and 120 km (marked as 5, and 6), respectively. In the height region below 95 km, T_e scatters and is not reliable because the measurement is done in the disturbed wake and the rocket surrounding is heated by aerodynamics.

3.2 Detail structure of N_e, T_e and electric field

Figures 4, 5, and 6 provide the fine structures of N_e, T_e, and the electric field at 6 points, which are mentioned in Sect. 3.1.

The N_e, T_e and electric field at three points 1, 2, and 3 are shown in three panels of Fig. 4. The numbers that are attached to each panel correspond to the points shown in Fig. 3.

As the bottom panel of Fig. 4 shows, N_e decreases at the height of 128 km and increases at the height of 128.8 km.

As in the case of sporadic E layer at the 100–110 km, which was discussed in another paper (Oyama et al., 2008), T_e shows anti-correlation with N_e. At the height of 127.7 km where N_e shows the minimum, T_e shows the maximum, and is 1000 K higher than that of ambient plasma at 126 km. The value is nearly 2 times of that at the height of 126 km. At the height of 128.8 km where N_e shows the maximum, T_e reduces. Inverse relation between N_e and T_e implies a heat source in the ionospheric E region even at night.

The electric field changes from southwest to east at the height of 126 km as the height changes from 125 km to 128 km, and shows the peak value of 8–9 mV/m at the height of 127.3 km. Difference in height exists between the peak of T_e, N_e minimum, and peak of the electric field.

In the middle panel of Fig. 4, N_e, T_e and electric field at the point 2 are shown. Nearly the same features as those at point 1 can be found, although they are not clear as point 1. N_e gradually reduces from 135 km, and takes the minimum at the height of 138.5 km. After N_e shows a small peak at 139.5 km, it gradually reduces toward the height of 143 km. T_e slightly increases from 135 km and takes a small peak at 138.5 km, then shows a lower value at 139.5 km. In the same way as at point 1, inverse relationship is again found between T_e and N_e. The electric field rapidly changes its direction from southwest to east in the height region of 137–139 km, and above that height the direction changes slowly toward southwest. The magnitude of the electric field shows the peak of 3.5 mV/m at 139 km. The height appears to correspond to the T_e maximum and N_e minimum.

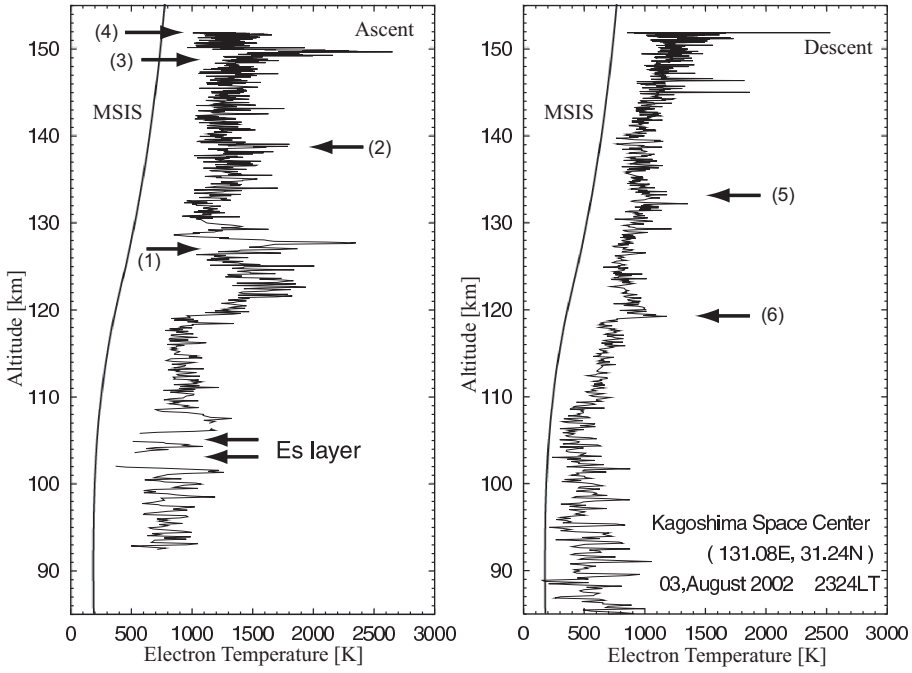

Fig. 3. Height profiles of electron temperature for ascent (left) and descent (right). Numbers indicated as 1–6 are the height regions which we discuss in Figs. 4, 5, and 6. Neutral temperature calculated from the MSIS-86 model is also indicated by a solid line. Scale for T_e is also applied to the neutral temperature.

The top panel of Fig. 4 shows the N_e, T_e and electric field at point 3. N_e gradually reduces from 148 km toward 149.5 km, takes the minimum at the height of 149.7 km. Between the height of 150–150.5 km, N_e appears to show a higher value that at 151 km; a small N_e peak exists at 150.5 km. T_e shows gradual increase toward 149.5 km, and the peak at 149.7 km. Peak T_e at 149.7 km is 2 times of T_e at the height of 148 km. At the height of 150.5 km, T_e appears to be the minimum. Again, as in the case of points 1, and 2, N_e and T_e show the inverse relation at point 3 as well. The electric field changes its direction from southwest to northeast in the height range of 146–148 km and from northeast to southwest at the height of 150 km. The peak intensity of the electric field, 7.5 mV/m is observed at the height of 149.6 km. This height appears to be different from the N_e minimum, and T_e maximum heights by about 0.1–0.2 km.

In Fig. 5, the same parameters are plotted for point 4. As this region is around the rocket apogee and the rocket height does not change so rapidly, the data is plotted versus time after the rocket launch at the left side of the figure and corresponding heights at the right. N_e gradually reduces from 185 s, and shows the minimum at 195 s. Between 200–205 s, N_e shows the broad peak. After the broad peak, N_e gradually reduces. T_e gradually decreases towards 193 s and shows the peak at 195 s. At 200 s and 205 s, T_e indicates small humps. The inverse correlation between N_e and T_e is seen at 195 s, and at 200–205 s. During 185–210 s, the electric field changes the direction from southwest, northeast, and then to northwest. The maximum intensity of the electric field of 4.7 mV/m appears at 201 s. However, this peak does not coincide with the T_e peak and N_e minimum at 195 s. It appears to agree with T_e peak, and N_e dip at 200 s.

Figure 6 shows the expanded height profiles of points 5 (upper panel), and 6 (lower panel). N_e shows a faint minimum at 134.5 km, and shows a peak at 135.4 km. Above 135.5 km, N_e shows a constant value of 1500 els/cm^3, indicates a small peak at 137 km, and gradually increases towards 139 km. Features, which appeared at points 1, 2, 3, and 4, are not clear at point 5. That is, T_e minimum, which is supposed to appear at the N_e maximum at 135.5 km, is not clear. The direction of the electric field gradually changes from west at 133 km to northwest at 136 km. Above the 136 km, the direction suddenly recovers to a westerly direction. The peak of the electric field is not observable. The behavior of the electric field is different from the cases 1, 2, 3, and 4.

At point 6, N_e gradually reduces towards 116.5 km, shows a peak at 118.2 km, and takes a minimum at 118.3 km. Above the height of 118.3 km, N_e gradually increases towards 124 km. T_e shows the broad maximum at 116 km, takes the minimum value at 118 km, and again illustrates the peak at 118.5 km. Above 118.5 km, T_e reduces toward 124 km.

The electric field shows an abrupt change in the direction from 115 km, points virtually east at 116.2 km, and stays in a southerly direction above 118 km.

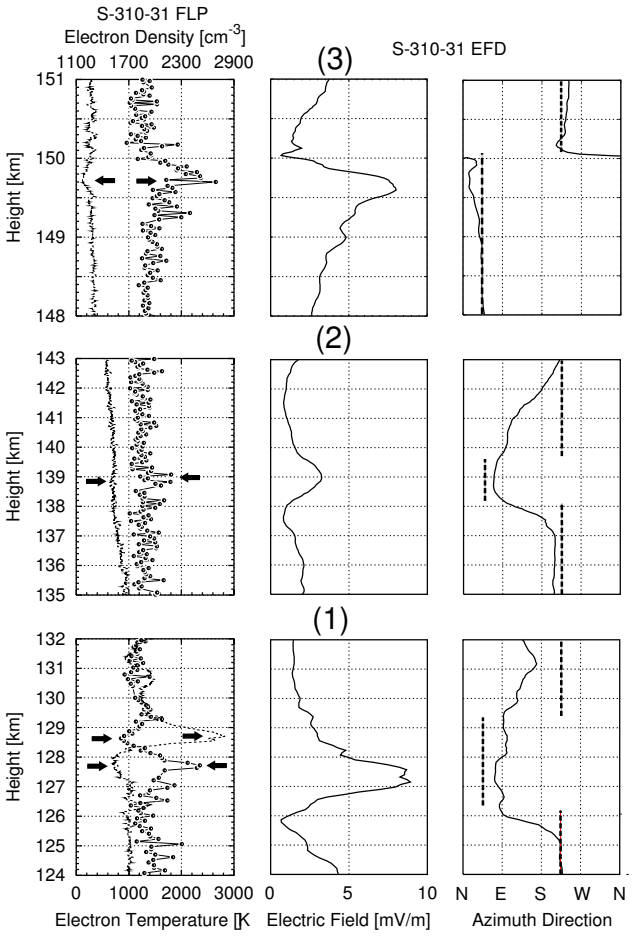

Fig. 4. Detailed structure of N_e (dot), T_e (squares connected with line) (left panel), and the electric field (thin lines) (right panel) at points 1, 2, and 3. In the right panel, direction of electric field, which is predicted from computer simulation by Yokoyama et al. (2004), is superimposed on the observed value by dashed line.

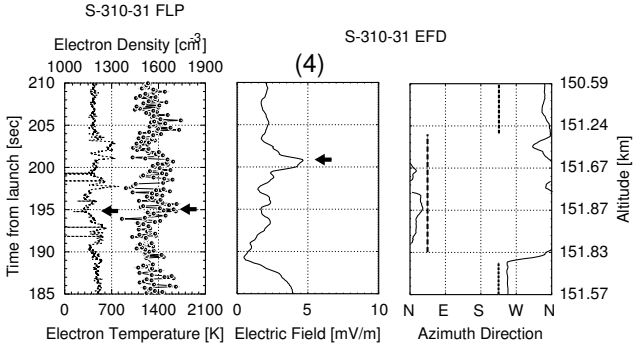

Fig. 5. Same as Fig. 4 but point 4. Direction of electric field, which is predicted from computer simulation by Yokoyama et al. (2004), is superimposed on the observed value by dashed line.

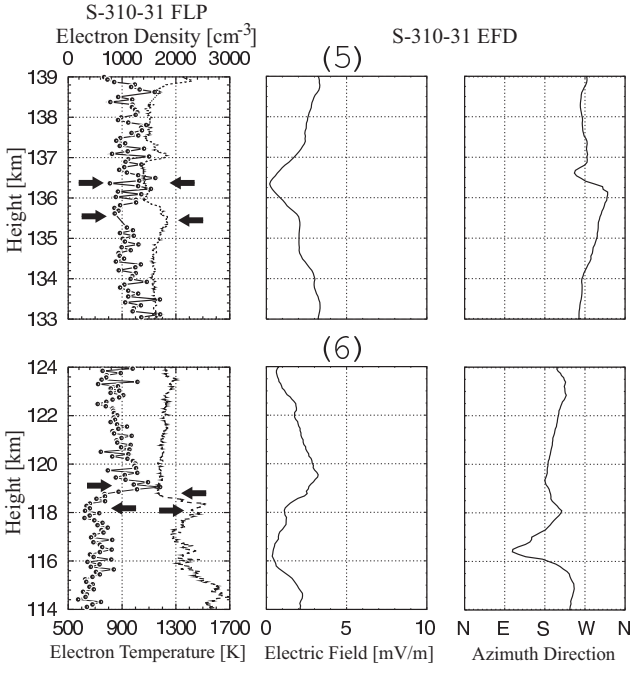

Fig. 6. Same as Fig. 4 but for points 5 and 6. Direction of electric field is not superimposed, because down leg data of N_e and T_e does not show clear common features that are revealed at points 1, 2, 3, and 4.

The description above is summarized in Table 1. Although, in the table, only the reduction of N_e is mentioned at the point of 2, 3, and 4, a small increase of N_e is also found at these points after the reduction of N_e similar to points 1, 5, and 6.

3.3 Energetics in the lower E region

Figure 7 shows energy densities of thermal electrons during ascent (left panel) and descent (right panel), that are calculated as ($N_e \times kT_e$, where k is Boltzmann constant).

In the ascent, minimum of energy density appears at the height of 107 km, where N_e shows the lowest. After the peak, which appears at the height of 109 km, the energy density gradually reduces with a small minimum at the height of 117 km. Above the height of 123 km, the energy density illustrates a small negative height gradient (or constant) up to the maximum altitude.

In the descent, below the height of 100 km, the value may not be accurate, because T_e is estimated higher than the true value due to the aerodynamic heating as we mentioned in Sect. 3. The profile shows a peak at the height of 102.2 km, and the second small peak at the height of 106 km, respectively. A small minimum is shown at the height of 108 km. Towards the height of 152 km, the energy density slowly reduces.

We conclude from Fig. 7 that (1) energy density in the height range of 100–110 km is higher than in other heights, and (2) it reduces towards both higher and lower altitudes

Table 1. Electron temperature, electron density, and electric field (peak value is referred to the value below the peak).

Region	Deviation of three parameters (height)		
	Electron temperature	Electron density	Electric field
1	+100% (127.7 km) −30% (128.8 km)	−10% (128.0 km) +60% (128.8 km)	5–9 mV/m (127.3 km) No peak
2	+40% (138.9 km)	−3% (138.9 km)	3 mV/m (138.6 km)
3	+100% (149.7 km)	−15% (149.7 km)	7–8 mV/m (149.7 km)
4	+13% (151.9 km)	−9% (151.9 km)	4.5 mV/m (151.6 km)
5	+10% (136.4 km) −8% (135.6 km)	−10% (136.4 km) +12% (135.5 km)	No Peak
6	+50% (119.0 km) −20% (118.0 km)	−20% (118.8 km) +30% (118.4 km)	3 mV/m (118.8 km) No peak

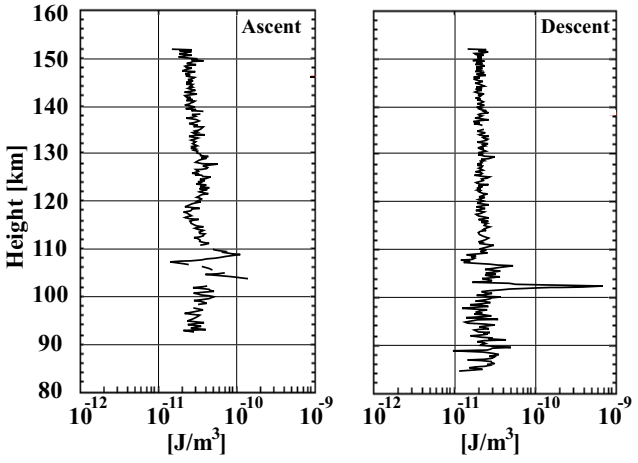

Fig. 7. Energy density of thermal electrons calculated from N_e and T_e. Note the small negative and positive height gradients, extending from the height of about 105 km to the higher and lower heights, respectively, which suggests the existence of some heat source around 105 km.

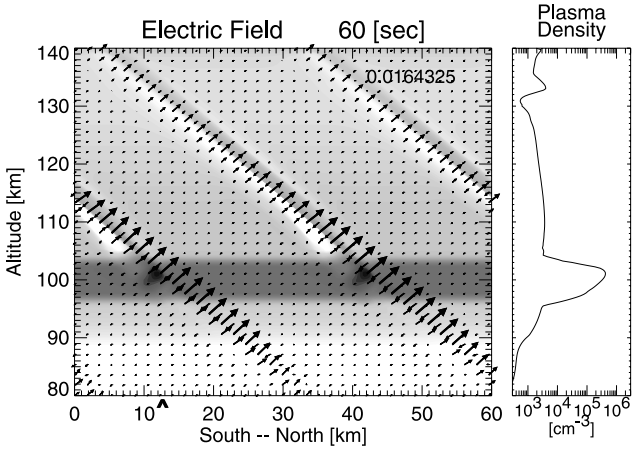

Fig. 8. Height profile of N_e and electric field, computed by Yokoyama et al. (2004). Note that N_e first drops at the height of 131 km, shows a peak at 133 km, and again drops at 135 km. This structure resembles the structures, which appear at points 1, 2, 3, and 4 in Figs. 4 and 5. Number 60 [s] at the top of the figure is the time after the initiation of computation, and number of 0.0164325 (16.4325 mV/m) shows the largest electric fields, which are shown in the figure by arrows.

from 100–110 km. This fact seems to suggest that heat source is confined to a height region where E_s appears.

3.4 Spatial structure of E_s

We speculate the 3-D structure of E_s by using T_e, N_e and electric field data, which were shown in Figs. 3, 4, and 5. We try to discuss our result by referring the result of computer simulation conducted by Yokoyama et al. (2003). The assumptions for the computer simulation are 1) Rod like E_s extends east-west direction at the height of 100 km, 2) Magnetic line of force has 45 degrees with respect to the ground, pointing from south to north, 3) Neutral wind blows from north to south with the maximum speed of 70 m/s around the height of 100 km, and 4) No external electric field is applied.

The 2-D structure of N_e and electric field around E_s resulting from the computer simulation is shown in Fig. 8, where N_e and the electric field are uniform in the direction vertical to the paper. The figure shows the followings.

The polarization of the electric field is produced at the boundary of rod-like E_s where strong gradient of N_e exists. As a result, a region of high N_e appears in the rod-like structure at the upstream of neutral wind. Inside the high-density region, plasma irregularities appear and the electric field is northward (opposite to the neutral wind direction). Low N_e region is produced in the downstream of neutral wind. In the background, which is far from the rod-like structures at 100 km, the electric field prevails in a southerly direction, which is the same direction as the neutral wind. In Figs. 4, and 5, the directions of electric field inferred from the computer simulation by Yokoyama et al. (2003), which shows the

Table 2. Comparison between observed features and those of model structure proposed by Yokoyama et al. (2004).

Parameters	Model*	Region 1	Region 2	Region 3	Region 4
Direction of neutral wind	SW	SSW	SSW	SSW	SSW
Variation of electric field	SW	SW (125 km)	SW (135 km)	SW (145 km)	SW (150 km)
	→NE	→E (128 km)	→E (138 km)	→NE (149 km)	→NE (151 km)
	→SW	→SE (142 km)	→S (142 km)	→SW (150 km)	→NW (151.5 km)
Variation pattern of N_e	Dec*	−10%	−3%	−15%	−9%
	→Inc*.	→+60%			

* SW, SSW, and NE: Southwest, Southsouth West, and Northeast
Variation of electric field: from lower altitude to higher altitude
Dec. and Inc for N_e: decrease and increase.

direction changes by 180° at the density perturbed region, are superimposed on the observed values. It is noted that the directions of the electric field measured at points 1, 2, and 3, agrees with the theoretical result.

The simulation suggests that a sheet-like structure extends along the magnetic filed line from the original rod shaped E_s.

We presume from the measurements of N_e, T_e and electric field that rod-like structure extends southeast/northwest with southwest neutral wind as shown in Fig. 9. Larsen et al. (2005) measured neutral wind by using TMA ejected from the rocket S-310-32, 15 min after the launch of S-310-31. The zonal and meridional winds are 10 m/s westerly and 40 m/s southerly at the height of 100 km, and reach 50 m/s and 80 m/s at 103 km, respectively. At the height of 105 km and 108 km, meridional wind becomes zero m/s. Between these heights the wind shows 50 m/s southerly at 106.3 km. Zonal wind shows 0 m/s at the height of 106.3 km and the velocity reaches 80 m/s westerly at the height of 108 km. On an average, the direction of neutral wind is between south and southwest.

Under the influence of the neutral wind, a sheet structure extending southeast/northwest along the geomagnetic line of force, is considered to be generated. The structure originates from the rod-like structure at the height of ∼105 km. N_e becomes lower at the southwest side and higher at the northeast side. The electric field inside the sheet is in a northeasterly direction and in other places the electric field should be in a southwesterly direction.

These features correspond to the result of Yokoyama et al. (2003), which is rotated at 45 degrees in the horizontal plane. It is presumed that the rocket went through the field-aligned sheet structure, which we described above. Then the behavior of the electric field, and electron density with respect to the height generally agrees with the features, which are derived from the computer simulation as we summarize in Table 2. The directions of theoretical electric field were already shown in Figs. 4 and 5. The spacing of two rod-like structures at E_s height is 13–14 km, which we can presume from the features observed at points 1, 2, 3, and 4.

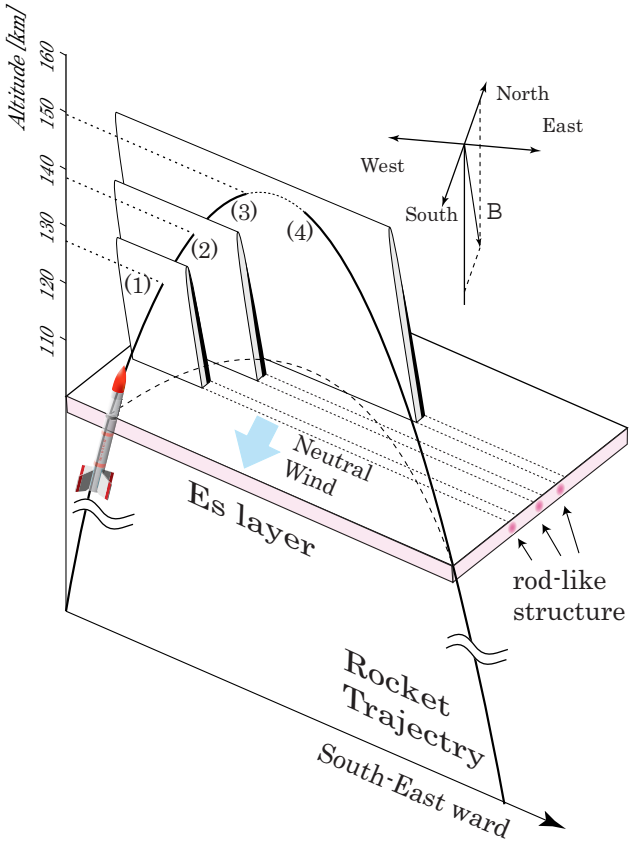

Fig. 9. Spatial structure of E_s, which is speculated from the measurement of T_e, N_e, and electric field. Numbers 1, 2, 3, and 4 correspond the heights, 128 km, 139 km, 149 km and 151 km which are mentioned in Figs. 3, 4, and 5. Distance between two rods, which is presumed from the rocket measurements, is 13–14 km at the height of 105 km.

4 Conclusions

We studied energetitcs and spatial structure of nighttime sporadic E layer in mid latitude by using N_e, T_e and electric

field data, which have been measured simultaneously on the same rocket. Good correlation between steep increase of T_e, N_e, and variation of electric field intensity seems to imply that there is additional heating source, which might be related to the sporadic E layer. The heat source which raises background T_e higher than neutral temperature in the lower E region (100–130 km) is still not identified.

We also tried to draw a 3-D picture of E_s, by using N_e, T_e, and electric field data by referring the computer simulation proposed by Yokoyama et al. (2003). The behavior of N_e and electric field show quantitative agreement between model and observation, although the agreement is not complete.

We showed here that a well prepared T_e measurement could give useful information to understand structure and energetics of E_s.

Acknowledgements. The authors express their sincere thanks to the rocket launch crews of the Institute of Space and Astronautical Science for their successful operation. They also express their gratitude to all government institutions and fishery Unions for their supports.

Topical Editor M. Pinnock thanks H. S. S. Sinha and another anonymous referee for their help in evaluating this paper.

References

Hedin, A.: MSIS-86 thermospheric model, J. Geophys. Res., 92(A5), 4649–4662, 1987.

Langmuir, I. and Motto-Smith, H.: Studies of electric discharges in gases at low pressures Part I–V, General Electric Rev., 28, 449–455, 538–548, 616–623, 762–771, 810–820, 1924.

Larsen, M. F., Yamamoto, M., Fukao, S., Tsunoda, R. T., and Saito, A.: Observation of neutral winds, wind shears, and wave structure during a sporadic-E/QP event, Ann. Geophys., 23, 2369–2375, 2005, http://www.ann-geophys.net/23/2369/2005/.

Oyama, K.-I. and Hirao, K.: Application of a glass sealed Langmuir probe to ionosphere study, Rev. Sci. Instr., 47, 101–107, 1976.

Oyama, K.-I., Abe, T., Mori, H., and Liu, J. Y.: Electron temperature in nighttime sporadic E layer at mid-latitude, Ann. Geophys., 26, 533–541, 2008, http://www.ann-geophys.net/26/533/2008/.

Pfaff, R., Freudenreich, H., Yokoyama, T., Yamamoto, M., Fukao, S., Mori, H., Otsuki, S., and Iwagami, N.: Electric field measurements of DC and long wavelength structures associated with sporadic-E layers and QP radar echoes, Ann. Geophys., 23, 2319–2334, 2005, http://www.ann-geophys.net/23/2319/2005/.

Saito, S., Yamamoto, M., Fukao, S., Marumoto, M., and Tsunoda, R. T.: Radar observations of field-aligned plasma irregularities in the SEEK-2 campaign, Ann. Geophys., 23, 2307–2318, 2005, http://www.ann-geophys.net/23/2307/2005/.

Schutz, S. R. and Smith, L. G.: Electron temperature measurements in mid-latitude Sporadic E layers, J. Geophys. Res., 81, 3214–3220, 1976.

Valenzuela, A., Bauer, O., and Haerendel, G.: Balloon observation of ionospheric magnesium ions, J. Atmos. Terr. Phys., 43, 785–788, 1981.

Yamamoto, M., Fukao, S., Tsunoda, R. T., Pfaff, R., and Hayakawa, H.: SEEK-2 (Sporadic-E Experiment over Kyushu 2) – Project Outline, and Significance, Ann. Geophys., 23, 2295–2305, 2005, http://www.ann-geophys.net/23/2295/2005/.

Yokoyama, T., Yamamoto, M., and Fukao, S.: Computer simulation of polarization electric field as a source of midlatitude field-aligned irregularities, J. Geophys. Res., 108(A2), 1054(SIA2), doi:10.1029/2002JA009513, 2003.